

Synchronous measurement of even and odd order intermodulation distortion at the resonant frequency of a superconducting resonator

Evan K. Pease^{1,3}, Bradley J. Dober^{2,3}, S.K. Remillard^{3,a}

¹*Department of Physics, Kenyon College, Gambier, OH, 43022, USA*

²*Department of Physics, University of Wisconsin, Madison, WI 53706, USA*

³*Physics Department, Hope College, Holland, MI, 49423, USA*

Abstract

A method has been developed which uses three input tones to measure both even and odd order intermodulation distortion (IMD) inside the pass band of resonant devices. With this technique the surface current density of both the driving signal and the IMD tones can be quantified. Synchronous, or same frequency, measurement of both even and odd order distortion permits quantitative comparison of the respective nonlinearity currents measured within the same timescale. As an example of this technique, a superconducting resonator is used to generate even and odd order IMD at the same frequency, resulting in physical conclusions which are pertinent to current research in high temperature superconductors. While varying the level of only one tone, the expected slope of the IMD current versus the driving signal current for both orders is unity, but that is only observed at high temperature when the superconductor becomes very lossy. An observed smaller slope at lower temperatures gives support to the linear-nonlinear interaction model. Also, a sharp increase in the 3rd order IMD relative to the 2nd order IMD near T_C gives support to a substantial nonlinear Meissner effect.

^aCorresponding author: TEL 616-395-7507, email remillard@hope.edu

I Background

Current flowing through a superconductor is commonly modeled as a two-component fluid with one component composed of paired charge carriers called Cooper pairs and the other component composed of unpaired charge carriers, called normal carriers. The Cooper pair current flows without electrical resistance and shunts the normal carriers. A kinetic inductance, $L_K = \mu_0 \lambda_L^2$, is associated with the Cooper pair movement, where μ_0 is the permeability of free space and λ_L is the London penetration depth. For current at microwave frequency, f , the inductive reactance, $2\pi \cdot f \cdot L_K$, of the Cooper pair current becomes significant enough that the normal carriers are no longer perfectly shunted and electrical loss can be detected despite the superconducting state of the material. Consequently, a microwave resonator fabricated from a superconductor has a finite peak width, providing a clear indication of dissipation.

The inductance of a superconducting thin film transmission line increases in the presence of a large amplitude microwave current. The origin of the nonlinear inductance can be intrinsic to the superconducting state as described by the nonlinear Meissner effect¹. Likewise, the origin of the nonlinearity can be extrinsic to the superconducting state from a variety of material related factors. For example, grain boundaries exhibit Josephson junction behavior, passing Cooper pairs at low amplitude microwave current, and breaking Cooper pairs at high amplitude microwave current as Josephson vortices nucleate in the grain boundaries. With such a nonlinear inductance, a large amplitude microwave current of frequency, f , incident on a superconducting transmission line will generate harmonic terms at $2f$, $3f$, $4f$, etc.

In order to relate the various intrinsic and extrinsic mechanisms to the observed nonlinearity, various authors^{2,3} have reported measurement of the harmonic emission from high-temperature superconductors. 2nd and 3rd order nonlinearity have uniquely different origins, with 2nd order thought to have extrinsic origins in the Josephson weak links especially at low temperature³. Third order nonlinearity has a significant intrinsic contribution from the nonlinear Meissner effect¹. Oates, et al.⁴ argued however that comparisons of the 2nd and 3rd harmonic emission from the superconducting device to the nonlinearity which is observed at the resonant frequency through the current dependence of the resonant peak width is not clearly useful due to the different time scales associated with the frequencies f , $2f$ and $3f$. Thus a method to measure nonlinearities of multiple orders at the same frequency has been developed and is reported here.

II Three-tone intermodulation distortion measurement

In order to examine the relative effects of even and odd order nonlinearity, 2nd and 3rd order harmonic distortion measurement has previously been used, with some theoretical explanation⁵ relating 2nd harmonic generation to vortex nucleation in weak links and 3rd harmonic generation to nonlinear junction impedance. However, intermodulation generation and harmonic generation of the same order should arise from the same nonlinear material properties (e.g. penetration depth and conductivity) since these nonlinearity terms result from the same term in the Taylor series expansion of the driving signals⁶ $H_1 \sin(2\pi f_1 t) + H_2 \sin(2\pi f_2 t) + \dots$. By removing device parameters and by scaling the frequencies of the nonlinearities, Booth, et al. demonstrated experimentally in Reference [6] that 3rd harmonic distortion and third order intermodulation distortion (IMD) are in fact equivalent for patterned thin film superconducting devices. Many authors^{7,8,9,10} report measurements of IMD on superconducting resonators made by introducing two signals, f_1 and f_2 , both inside the resonant peak and detecting mixing terms at, for example, $2f_2 \pm f_1$, also inside the resonant peak. The second order intermodulation terms at $f_1 \pm f_2$ are far

outside the resonant peak, and do not address the issue of electrodynamic time scale raised by Oates. By using signals with three different frequencies, it is possible to realize both even and odd order nonlinearity at the same frequency and also with the same strength of coupling to a detection probe placed near the resonator. Three tone IMD measurements were previously done by one of the authors (SKR) to find third order IMD occurring in the pass band of high-temperature superconducting (HTS) filters¹¹.

The 3rd order nonlinearity of the folded superconducting resonator design shown in Figure 1 has been previously studied by Zhuravel, et al¹². The 400 nm thick $Tl_2Ba_2CaCu_2O_8$ structure on a Lanthanum Aluminate substrate was designed and patterned by ISCO International, Inc. of Louisville, CO for use in wireless telecommunications filters. Its fundamental resonant frequency at 78 K is 912.0 MHz, and with the probes in place it has a loaded peak width at low input power of about 200 KHz and an unloaded Q of about 7,000. The fundamental mode will be used for the characterization reported here.

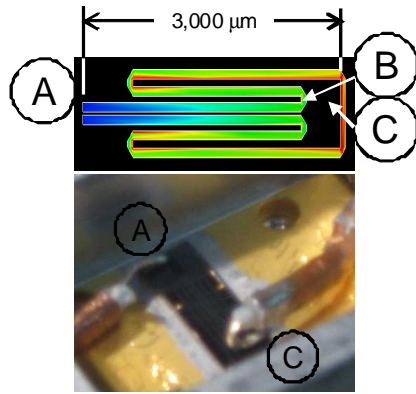


Figure 1. (top) Simulation of the current distribution at resonance for the structure used in this work. (bottom) The superconducting resonator chip with the couplers shown at Points A and C. The third coupler is attached to the lid of the housing, so it is not visible in the photo.

The three signals are introduced into the resonator in two different locations, using two different probes. The *probing* signals f_1 and f_2 are introduced by a magnetic dipole probe placed at Point B in Figure 1. The *driving* signal f_3 is introduced by a magnetic dipole probe placed at Point C. Better probe isolation can be achieved by using the electric probe for the probing signals since electric and magnetic probes are known to exhibit extremely weak cross-coupling, but this isolation has been unnecessary with suitable filtering. The IMD signals and the transmitted drive signal are detected by an electric monopole probe, which in Figure 1 is located at Point A. Using two separate input antennae for the out-of-band probing signals and the in-band driving signal avoids the need for ultra-broadband isolated combiners prior to introduction into the resonator, and more importantly virtually eliminates any possibility of the measured IMD being generated in the signal generators or in the coupling structures.

The electric monopole and magnetic dipole probes, at Points A and C in Figure 1 respectively, are formed from the center conductor of 0.086 inch semi-rigid coaxial cable, which has a wire diameter of 0.5 mm. The magnetic dipole loop has a diameter of about 2.5 mm.

Opportunity for miniaturization with this type of probe construction is available by using 0.020 inch semi-rigid coaxial cable which has a center conductor diameter of 0.11 mm.

In one particular exercise of this method, three signals were introduced into the resonator at $f_1=90$ KHz, $f_2=200$ KHz and $f_3=911.9$ MHz. With these three frequencies, second order IMD is emitted at $f_3+f_1= 911.99$ MHz and third order IMD is emitted at $f_3+(f_2-f_1)=912.0$ MHz. Given the 3 dB width of the loaded resonance peak of about 300 KHz, these frequencies are essentially identical and are situated at the resonant frequency. Using a sufficiently low resolution bandwidth (RBW=10 Hz), a spectrum analyzer is easily able to resolve these nonlinearity tones.

The configuration of test equipment and test components is shown in Figure 2. The probing signals, f_1 and f_2 are combined with a Merrimac model PD-20-10 lumped element isolated power combiner (3). The 20 dB of signal generator isolation provided by the combiner (3) is essential because high reverse power into the signal generators induces gain compression in the generator output. Mixing of the signals f_1 and f_2 at the frequency of the IMD is not a concern due the orders of magnitude frequency difference between the probing frequencies and the IMD frequency. It is especially important to isolate the signal generator producing the drive signal, f_3 , as the power level at this frequency is the independent variable in the experiment. In the event that reflected power at f_3 causes the generator which produces f_3 to go into compression, a ferrite isolator (2) should be placed on the output port of the generator. A 900 MHz bandpass filter (4) and a 400 MHz low pass filter (5) protect the probing signal generators and the driving signal generator from cross-coupling which would produce unwanted system intermodulation distortion at the IMD test frequency. The low pass filter (5) also ensures that in-band mixing terms from the probing signal generators do not arrive at the device under test (6).

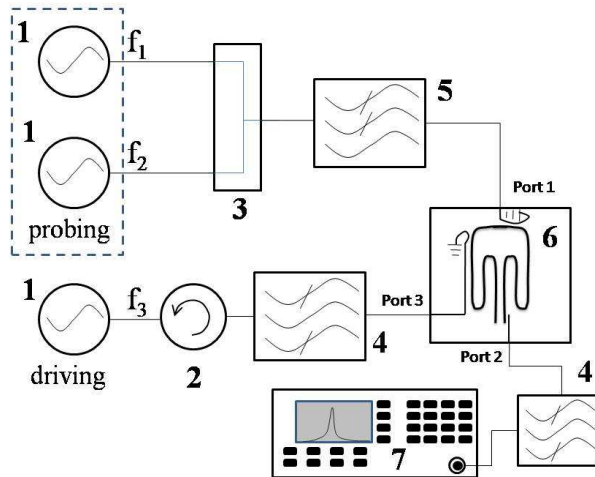


Figure 2. A driving signal at f_3 and two low frequency probing signals, f_1 and f_2 are fed into the device under test (6) after passive conditioning with a UTE Microwave CT-1395-NT ferrite isolator (2), a Merrimac PD-20-10 lumped element isolated combiner (3), a band pass filter (4) and a 400 MHz low pass filter (5). The output of the DUT is further cleaned with an optional band pass filter before entering the HP8566B Spectrum Analyzer (7). f_1 and f_2 were generated by an Agilent 8648C signal generator and a Rhode & Schwartz SMB100A Signal Generator respectively. f_3 was generated with an Agilent E4421B Signal Generator with frequency sweeping capability.

The probing and driving signals are fed directly into the superconducting device without combining. As depicted in Figure 2, magnetic dipole antennae are used to couple the driving and probing signals into the device under test (6) and an electric monopole antenna is used to couple signal out. Dependence of the IMD on the presence of the driving signal, f_3 , ensures that the IMD is in fact three-tone mixing, and not an artifact of mixing between the two probing signals. An electric monopole could also be used to introduce the probing signals. In one potential realization of this technique, a movable electric monopole antenna brings in the probing signal which then would result in a spatial scan of the even and odd order nonlinearity across the sample.

The probing signals are significantly attenuated (usually by about 100 dB) at Port 2 because they are not resonant with the device. The drive signal and the IMD signals are both detected with the probe at Port 2. Another 900 MHz bandpass filter (4) can be placed at the output of the device under test if it is found that the probing signal level coupled out is sufficient to generate IMD in the hp8566B Spectrum Analyzer (7). This has not been found to be necessary at the probing power levels used here.

III Analysis of the output signals

In order to draw quantitative conclusions about the superconductor electrodynamics revealed by detected IMD, it is essential to correlate the electric current in the superconductor at the IMD frequency to the current at the drive frequency. Similarly, Lee, et al.¹³ used the current density stored in the 2nd harmonic emission relative to the current density stored in the 3rd harmonic emission to determine the portion of the current density that was breaking time reversal symmetry. When used along with an electromagnetic field simulator, the configuration in Figure 2 allows the quantitative determination of current in the fundamental resonance as well as the current that produces the IMD signals. IE3D method-of-moments software from Zeland Software¹⁴ was used to compute the current density that corresponds to a particular dissipated power.

Determination of surface current

The circuit in Figure 2 provides a measurement of the 2nd and 3rd order intermodulation distortion power, both of which are at the same frequency, versus the driving signal power. However, the raw IMD power is not indicative of the change in coupling into the resonator that occurs as the input power changes. Nor does it reveal the fundamental dependence of nonlinearity on the current. For example, Remillard¹⁵ reported 2-tone and 3-tone IMD measured on electrically identical HTS filters made with either thin film or thick film HTS materials. The thick film filters generated lower IMD, even though the material quality was far worse. The lower current density in the thick film structures was responsible for this distinction. Although that study satisfied its engineering objective of comparing the two types of devices, in order to study the electrodynamics of nonlinear materials, it is more useful to acquire a quantitative measure of the surface current density, K (Amps/meter), which produces the measured IMD power.

Current density is not usually measured in passive microwave devices, but the power dissipated, P_{diss} , in the device can be readily measured. In a superconducting microstrip resonator, power is dissipated in the dielectric substrate, P_{dieb} , and in the superconductor, P_s ,

which is composed of the microstrip line and the ground plane. The dissipated power is thus written as $P_{diss}=P_S+P_{diel}$. The power dissipated in the superconductor is found by integrating the magnetic field, H , and the superconductor's surface resistance, R_S , over the surfaces of the superconductor¹⁶, $P_S = \frac{1}{2} \iint R_S \vec{H} \cdot \vec{H}^* ds$, where the asterisk indicates complex conjugate. The power dissipated in the dielectric is $P_{diel}=(\text{circulating power})/(\text{dielectric } Q)=(2\pi f \cdot U) \cdot f_d \tan \delta$, where U is the stored energy, f_d is the dielectric filling factor and $\tan \delta$ is the loss tangent of the dielectric. Since the partial Q of the superconductor is $Q_S=G/R_S=2\pi f \cdot U/P_S$, circulating power, $2\pi f \cdot U$, is equally well known from the dissipation in the superconductor from $2\pi f \cdot U=P_S \cdot G/R_S$, where G is the geometry factor of the microstrip line. So $P_{diel}=P_S \cdot G \cdot f_d \cdot (\tan \delta)/R_S$. When the current handling materials in the device are linear, particularly when R_S is independent of current, the total dissipated power depends upon the surface current density through

$$\begin{aligned}
 P_{diss} &= \left[\frac{1}{2} \iint_{\text{surface}} R_S \vec{H} \cdot \vec{H}^* dS \right] \cdot \left[1 + \frac{G}{R_S} f_d \tan \delta \right] \\
 &= A R_{S,eff} K_{\max}^2 \cdot \left[1 + \frac{G}{R_S} f_d \tan \delta \right]
 \end{aligned} \tag{1}$$

$R_{S,eff}$ is the effective surface resistance and its use acknowledges both that R_S could have different values throughout the sample and that in the case of electrically thin films, R_S is influenced by the substrate. The geometry factor, G , was determined using IE3D to be 0.74Ω for the fundamental resonance. The filling factor, f_d , for the dielectric substrate, which in this case is lanthanum aluminate (dielectric constant at 78 K of about 23.9)¹⁷ was found using IE3D to be 0.977. f_d indicates the fraction of electric field energy confined to the dielectric. The loss tangent, $\tan \delta$, of lanthanum aluminate at cryogenic temperatures¹⁷ and 1 GHz is on the order of or less than 1.0×10^{-5} .

The first bracket in the first line of Equation (1) is the power dissipated in the superconductor. The second bracket is close to unity, with the product $(G/R_S)f_d \tan \delta$ being small (<0.1) and by application of the binomial expansion theorem therefore equivalent to the ratio of power dissipated in the dielectric to the power dissipated in the superconductor.

Surface current density, K , and magnetic field, H , are numerically equal, though perpendicular in relative orientation. When the material is nonlinear, R_S depends on the magnetic field at the surface, H . If the effective surface resistance is known from Q measurement and the proportionality constant in Equation (1) is determined numerically, then the peak surface current density in the resonator, K_{\max} , can be determined. IE3D was used to determine the constant of proportionality. In the case of the fundamental resonance of the structure in Figure 1, the constant of proportionality was found to be

$$A = (1.3 \pm 0.3) \times 10^{-4} \text{ m}^2 \tag{2}$$

where an uncertainty of 20% corresponds to a 1 dB confidence in the peak current determination using field simulation and stems from the coarse estimate of peak surface current at the corners of the patterned resonant structure. In most scientific inquiries, the relative strengths of K_{\max} for the various orders of nonlinear distortion are the quantity of interest, as well as their magnitudes

relative to the driving surface current density, meaning that the large uncertainty in the proportionality constant will not present a barrier to reaching many scientific conclusions from the measurements.

Measurement of the dissipated power

Given a value for the proportionality constant, A , a measurement of the dissipated power in the resonator results in a value generated for K_{max} by Equation (1). To compute the dissipated power, measurements need to be made of the reflection coefficients and loaded Q , $Q_L = \Delta f / f_r$, where f_r is the resonant frequency and Δf is the 3 dB full width at half maximum of the peak. Normally one might choose to use a network analyzer to make these measurements, but since knowledge of f_r and Δf is needed at each measurement point, the measurement was done using the sweeping capability of the Agilent E4421B Signal Generator, which produces the driving signal, along with an HP 8466B Spectrum Analyzer. Sweeping around resonance allowed the measurement of the 3-dB peak width. Reflection coefficients are measured by inserting a directional coupler at the resonator port and terminating the other ports as shown in Figure 3.

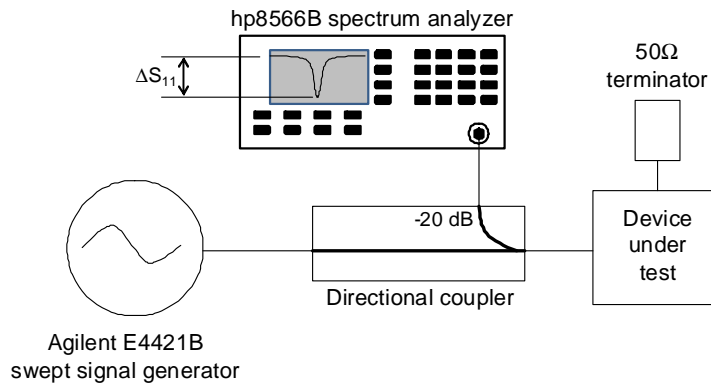


Figure 3. Measurement of the power reflected from the devices under test using a -20 dB M/A-COM KS-21603L7 directional coupler. ΔS_{11} from port 1, and ΔS_{22} from port 2, are used in Equation 3 to compute the reflection coefficients.

Using scattering parameters, the depth in decibels of the resonance in the reflected signal, ΔS_{11} or ΔS_{22} , yields the reflection coefficients. Provided the coupling at Port 3 is weak ($\Delta S_{33} < 1$ dB when low pass filter (5) is absent) then Port 3 can be left out of the coupling coefficient calculations, allowing this to be treated as a two-port problem. Support for tolerating a rather intrusive probe at Port 3 is seen in simulation with IE3D which showed that the presence of the low pass filter (5) ensures that even a very large value of ΔS_{33} while Port 3 is matched to 50Ω does not affect the power flowing into and out of Ports 1 and 2. In other words, S_{21} is not affected by the probe at Port 3 provided the low pass filter (5) is in place. This condition should also be assured to avoid strong field perturbation by the probe at Port 3. Since the probing signals introduced by this probe are not resonant, strong coupling of this probe at resonance is not essential. The coupling coefficients are computed from the reflected signals shown in Figure 3 with¹⁸

$$\beta_1 = \frac{1 - 10^{-\Delta S_{11}/20}}{10^{-\Delta S_{11}/20} + 10^{-\Delta S_{22}/20}} \quad \text{and} \quad \beta_2 = \frac{1 - 10^{-\Delta S_{22}/20}}{10^{-\Delta S_{11}/20} + 10^{-\Delta S_{22}/20}} \quad (3)$$

where ΔS is a positive number in decibels. The tedious reflection measurement only needs to be performed once. Although ΔS_{11} and ΔS_{22} depend on the resonator Q , which in turn depends on power and temperature, the external Q is a constant, allowing the reflection coefficients to be scaled from an original loaded Q value, Q_L^{old} , to any new loaded Q value, Q_L^{new} , through¹⁹

$$\beta_i^{\text{new}} = \frac{\beta_i^{\text{old}} Q_L^{\text{new}}}{(1 + \beta_i^{\text{old}}) Q_L^{\text{old}} - \beta_i^{\text{old}} Q_L^{\text{new}}} \quad (4)$$

where $i=1$ or 2 . Given values for the loaded Q , the unloaded Q , and the Port 1 and Port 2 coupling coefficients, the dissipated power can be computed from²⁰

$$P_{\text{diss}} = 4P_{\text{av}} \frac{\left(\frac{Q_L}{Q_u}\right) \left(1 - \frac{Q_L}{Q_u}\right)}{1 + \frac{\beta_2}{\beta_1}} \quad (5)$$

where P_{av} is the available power incident on Port 1, measured in Watts. $Q_u = Q_L(1 + \beta_1 + \beta_2)$ is the unloaded Q and represents the Q the resonator would have if it were isolated from its coupling ports.

The surface resistance used in Equation (1) is related to the measured Q value through²¹

$$R_s = G \left(\frac{1}{Q_u} - f_d \cdot \tan \delta \right). \quad (6)$$

Equations 1 through 6 are combined in a single step to compute the peak surface current density, K_{max} , from measured S-parameters. Figure 4a shows the peak surface current density versus the measured output power in Watts for the driving signal. This curve is straight forward to generate from measurement and readily fits a power law

$$K_{\text{max}} = B \cdot P_{\text{out}}^n \quad (7)$$

where B and n are fit parameters and P_{out} is the level of the driving power in Watts that comes out of Port 2. For all data sets, n is very close to 0.5 as expected. The data in Figure 4a include the power law fit to the form in Equation 7, performed using Origin, Version 8.0²².

Once the parameters in Equation 7 are known, Equation 7 can then be applied to the measured 2nd and 3rd order IMD signal power, also measured at Port 2. From this, the surface current density that produces the IMD signal is known. This relies on an assumption that the current distribution of the IMD signal follows the same transverse electromagnetic field distribution as the current. This assumption is supported by the laser scanning microscopy results of Zhuravel²³ using the same resonator design as in Figure 1, demonstrating that the 3rd

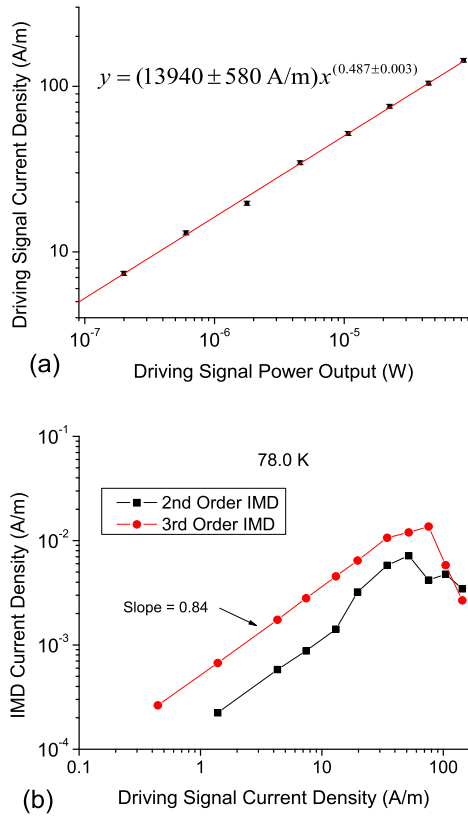


Figure 4. (a) Calibration of surface current density to the measured output power at 78.0 K. (b) 2nd and 3rd order IMD curves, both exhibiting a slope less than unity, even for a driving current density below 50 A/m.

temperature continued to increase. Signals at microwave frequencies see a lower transition temperature than direct current because of the temperature dependence of the pair breaking frequency. Above T_C , the thin film resonator had a Q of 35 and a center frequency of 890 MHz. The resonator was connected to a 25 Watt heater and placed inside a liquid nitrogen cooled cryostat. The temperature was monitored by a silicon diode and controlled with a Lakeshore model 330 Autotuning Temperature Controller. The source power at f_1 and f_2 was kept fixed at +10 dBm. The source power at f_3 , labeled P_3 , was varied from -40 dBm, to +10 dBm.

Measurements performed at 78.0 K are shown in Figure 4 using a two step test protocol. (i) The carrier power coming out of the resonator, P_{out} , is measured along with Q_L , and f_r over the 50 dB range of P_3 . The peak surface current, K_{max} , for the driving signal at f_3 is then computed using Equation (1). The dependence of this quantity on P_{out} is shown in Figure 4a. A power law fit to these data is then used to determine the fit parameters in Equation (7). (ii) The drive frequency, f_3 is then set such that the 2nd order IMD occurs at f_r . For example, if $f_1=500$ KHz,

order IMD was generated by currents whose peaks were co-located with the fundamental. Results from Hu²⁴ indicate though that although the 3rd order IMD current has a peak in the same location as the fundamental, the contrast in the current distribution may be different, leaving some open question about the assumption used in this work that the coupling coefficients measured using the resonance are applicable to the in-band IMD. But in these measurements, the 2nd and 3rd order IMD are locally generated by non-resonant signals introduced at Port 3. The nonlinear material at the location of the probe from Port 3 functions as a local signal generator, which then excites the resonance. Therefore, in the method of this paper, the measured IMD signal is in fact the resonance of the structure being excited by the local in-band nonlinearity. The coupling coefficients obtained from the resonance sweep pertain equally well to the IMD signal.

IV Synchronous intermodulation distortion measurements

The 400 nm thick $Tl_2Ba_2CaCu_2O_8$ thin film was patterned by argon ion beam milling on a 0.50 mm thick LAO substrate coated on both sides to provide a superconducting ground plane. The superconductor had a microwave transition temperature, T_C , of 102 K, as determined by the temperature where the Q no longer dropped as the

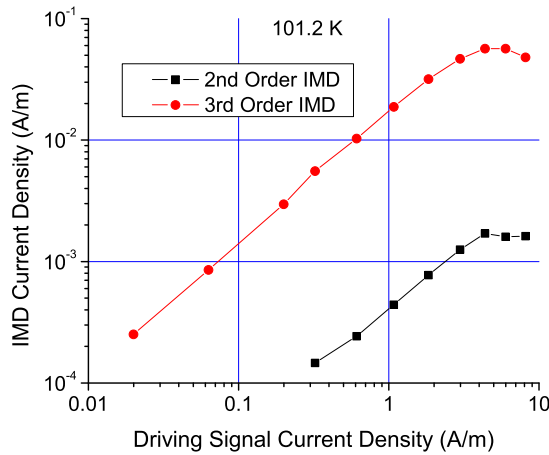


Figure 5. Close to T_C the third order IMD at 101.2 K has become considerably larger than the second order IMD, and both curves exhibit a slope of unity as expected.

expected. At 78.0 K the slope of the 2nd order IMD in Figure 4b is 0.82 and the slope of the 3rd order IMD is 0.84. Quite frequently superconducting devices exhibit non-ideal slopes resulting in a variety of phenomenological explanations. Recently, Henrie, et al.²⁵, developed a general model of linear-nonlinear component interaction to demonstrate that non-ideal IMD slopes are to be expected when dissipation occurs in a combination of linear and nonlinear devices. At 78.0 K where Q_u ranges from 2,000 to 8,000, between 1% and 8% of the drive current is dissipated in the non-superconducting linear substrate, depending on the amplitude of the driving current. At 101.2K, where Q_u varies from 80 to 200, essentially all of the dissipation (>99.8%) is in the nonlinear superconductor. As shown in Figure 5, the slopes for both orders are unity (actually 1.02 ± 0.02) at 101.2K where all of the dissipation is in nonlinear material.

Intrinsic nonlinearity is readily detected using three-tone intermodulation distortion. Close to T_C , the 3rd order IMD has grown considerably from its value at 78.0 K as also seen by other authors²⁶ and in keeping with the nonlinear Meissner effect. The 2nd order nonlinearity is seen to be considerably smaller than the third order nonlinearity, as was also found by Lee, et al.¹² using 2nd and 3rd order harmonic distortion.

Measurement Uncertainty and Systematic Errors

Both random and systematic errors play a role in the uncertainty of these measurements. The measurement precision of the IMD signal level using the service center calibrated hp 8566B Spectrum Analyzer is ± 0.1 dB, or $\pm 2\%$, with the smallest measurable quantity being about -130 dBm or 0.1 femto-Watt. Three tone IMD measurements are reproducible with complete system teardown to within ± 1.6 dB¹¹.

The determination of surface current density is less clearly known, primarily due to the uncertainty in the coefficient, A , estimated in Equation 2. In many cases, the ratio of K_{\max} in the 3rd order to K_{\max} in the 2nd order is the primary objective¹³, resulting in a cancellation of this

and $f_1=910.0$ MHz, then f_3 is set to 909.5 MHz. After the 2nd order IMD is measured, the drive frequency is moved slightly so that the 3rd order IMD occurs at f_r . For example if $f_2=700$ KHz, then f_3 needs to be set to 909.8 MHz so that 3rd order IMD occurs at $[909.8 + (700 \text{ KHz} - 500 \text{ KHz})]=910.0$ MHz. The 2nd and 3rd order IMD emitted by the resonator are used with Equation 7 along with the fit parameters to compute the peak current in the resonator associated with each IMD order. The dependencies of the peak currents of each IMD order upon the current of the driving signal at 78.0 K are shown in Figure 4b. In the range where IMD is dropping with increasing power, the S-parameter transmission peak becomes noticeably distorted from a Lorentzian.

Because only one input tone is being varied, a slope of unity for both orders is

systematic error since the coefficient, A , cancels with itself and thus does not even need to be known when the ratio is computed. An additional source of systematic error comes from the fit uncertainty in Figure 4a. This becomes a systematic rather than a random error because the fit parameters are then applied in the same manner to all data points. However, again in the event that the ratio of currents is what is being considered, the systematic errors cancel since the coefficient, A , cancels.

Miscalculation of the surface current could also result from the influence of the coupler at Port 3. This measurement depends on Equation 5 correctly returning a value for dissipated power. Calculation of dissipated power using Equation 5 assumes that the resonator is a two-port device. This assumption could break down if power is lost through Port 3. However, because of the low pass filter attached to Port 3, the transmission line from Port 3 is perfectly unmatched at resonance, reflecting all power back to the resonator. Simulation in IE3D with a third coupler in fact revealed that ΔS_{11} and ΔS_{22} are not affected to within ± 0.1 dB by the third coupler provided it is terminated with an out-of-band filter. In the simulations first performed without the Port 3 filter, the third coupler was moved progressively closer to the resonator until $\Delta S_{33}=8$ dB. Although ΔS_{11} and ΔS_{22} were severely affected, they returned to their unperturbed values when the filter was added.

V Conclusion

Three tone IMD has been used to measure even and odd order nonlinearity occurring at the same frequency. Sweeping over 5 orders of magnitude in input power, or 2.5 orders of magnitude in driving current, reveals the levels of 2nd and 3rd order IMD, their relative strengths, and their power law slopes relative to the driving signal. All observations lend insight into the phenomenology of superconductor nonlinearity. The slopes approach an ideal value of unity at high temperature, as expected from the linear-nonlinear interaction theory. Also, close to the transition temperature, the third order IMD rises relative to the 2nd order IMD, as expected by the nonlinear Meissner effect. Applications of this method can be pursued for other nonlinear materials. Although the approach put into practice here used a resonant sample, it is conceivable to devise a variation of this technique for unpatterned, hence non-resonant, magnetic thin films. Perhaps the most intriguing application of this technique could be realized by configuring Port 3 to be moveable, resulting in a scan across the sample of its 2nd and 3rd order microwave nonlinearity.

VI Acknowledgements

One of the authors (SKR) had useful discussions with Steven Anlage of the University of Maryland. The resonator tested in this paper was designed and fabricated by engineers at ISCO International in Louisville Colorado, with some key contributions from Jonathon Scupin. This work is being supported by a Cottrell College Science award from the Research Corporation, by Mesaplexx, pty. ltd. of Eight Mile Plains, Australia, and by the Hope College Natural and Applied Sciences Division. This material is also based upon work of two of the authors (EKP and BJD) which was supported by the National Science Foundation under NSF-REU (Research Experiences for Undergraduates) Grant to Hope College No. PHY-0452206.

References

- ¹ D. Agassi and D.E. Oates, Phys. Rev. B. **72**, 014538 (2005).
- ² G.Hempel, B.Batlogg, K.Krishana, N.P.Ong, W.Prusseit, H.Kinder, and A.C.Anderson, Appl. Phys. Lett. **71** 3904 (1997).
- ³ Y.M.Habib, C.J.Lehner, D.E.Oates, L.R.Vale, R.H.Ono, G.Dresselhaus, and M.S.Dresselhaus, Phys.Rev. B **57**, 13833 (1998).
- ⁴ D.E. Oates, S.-H. Park, M.A. Hein, P.J. Hirst and R.G. Humphrey, IEEE Trans. Appl. Supercond. **13**, 311 (2003).
- ⁵ J. McDonald and John R. Clem, Phys. Rev. B **56**, 14723 (1997).
- ⁶ James C. Booth, Kenneth Leong, Susan A. Schima, C. Collado, J.M. O'Callaghan and J. Mateu, J. Supercond. and Novel Magnetism **19**,531 (2006).
- ⁷ J.C.Booth, L.R.Vale and R.H.Ono, Physica C **357-360**, 1516 (2001).
- ⁸ H.Xin, D.E.Oates, G.Dresselhaus and M.S.Dresselhaus, Phys. Rev. B **65**, 214533 (2002).
- ⁹ G.Cifariello, M.Aurino, E.Di Gennaro, G.Lamura, P.Orgiani, J.-C.Villégier, X.X.Xi, and A.Andreone, 7th European Conference on Applied Superconductivity, J.Phys:Conf.Series, **43**, pp.702-705 (2006).
- ¹⁰ Stephen K. Remillard, Amr Abdelmonem, Piotr O. Radzikowski, Nick D. Lazzaro, and David S. Applegate, J. Superconductivity: Incorporating Novel Magnetism, **14**, 47 (2001).
- ¹¹ S. K. Remillard, H.R. Yi and Amr Abdelmonem, IEEE Trans. on Applied Supercond., **13**, 3797 (2003).
- ¹² Alexander P. Zhuravel (presenting author), Stephen Remillard, Steven M. Anlage, Alexey V. Ustinov, Kharkov Symposium on Physics and Engineering of Microwaves, Millimeter, and Submillimeter Waves (MSMW'04), Kharkov, Ukraine, 2004.
- ¹³ Sheng-Chiang Lee, Matthew Sullivan, Gregory R. Ruchti, Steven M. Anlage, Benjamin S. Palmer, B. Maiorov, and E. Osquiguil, Phys. Rev. B, **71**, 014507 (2005).
- ¹⁴ Zeland Software, Fremont, CA, USA.
- ¹⁵ S.K. Remillard and S. Cordone, J. Supercond.: Incorporating Novel Magnetism, **19**, 523 (2006).
- ¹⁶ John David Jackson, *Classical Electrodynamics, 2nd Edition* (Wiley, 1975), Chapter 8.
- ¹⁷ Claudio Zuccaro, Michael Winter, Norbert Klein, and Knut Urban, J. Appl. Phys., **82**, 5695 (1997).
- ¹⁸ Zhi-Yuan Shen, *High-Temperature Superconducting Microwave Circuits*, (Artech House, Norwood, MA, 1994).
- ¹⁹ S.K. Remillard, L.J. Klemptner, J.D. Hodge, T.A. Freeman, P.A. Smith, and T.W. Button, in High-Temp. Microwave Superconductors and Applications, James D. Hodge, editor, Proc. SPIE 2559, pp.59-68 (1995).
- ²⁰ *Reference Data for Radio Engineers, 6th Edition*, (Howard W. Sams and Co., Indianapolis, 1975), Chapter 24.
- ²¹ M. Hein, *High-Temperature-Superconductor Thin Films at Microwave Frequencies*, (Springer, Berlin, 1999), p. 49.
- ²² OriginLab Corporation, Northampton, MA, USA.
- ²³ Alexander P. Zhuravel, Steven M. Anlage, Stephen Remillard, and Alexey V. Ustinov, MSMW-07 Symposium Proceedings, Karhkov, Ukraine, July 2007.
- ²⁴ Wensheng Hu, A.S. Thanawalla, B.J. Feenstra, F.C. Wellstood, and Steven M. Anlage, Appl. Phys. Lett., **75**, no. 18, 2824, (1999).
- ²⁵ Justin Henrie, Andrew Christianson, and William J. Chappell, Appl. Phys. Lett., **94**, 114101 (2009).
- ²⁶ D. E. Oates, S.-H. Park, D. Agassi, and G. Koren, Supercond. Sci. Technol. **17**, 290 (2004).